Molecular Biology of the Cell
Vol. 18, 3302–3312, September 2007

Modulation of Proteinase K-resistant Prion Protein in Cells and Infectious Brain Homogenate by Redox Iron: Implications for Prion Replication and Disease Pathogenesis[D]

Subhabrata Basu,*† Maradumane L. Mohan,*† Xiu Luo,*† Bishwajit Kundu,‡ Qingzhong Kong,* and Neena Singh*

*Department of Pathology, Case Western Reserve University, Cleveland, OH 44106; and ‡Department of Biochemical Engineering and Biotechnology, The Indian Institute of Technology, New Delhi, India 110016

Submitted April 9, 2007; Revised May 31, 2007; Accepted June 4, 2007
Monitoring Editor: Jonathan Weissman

The principal infectious and pathogenic agent in all prion disorders is a β-sheet–rich isoform of the cellular prion protein (PrP^C) termed PrP-scrapie (PrP^{Sc}). Once initiated, PrP^{Sc} is self-replicating and toxic to neuronal cells, but the underlying mechanisms remain unclear. In this report, we demonstrate that PrP^C binds iron and transforms to a PrP^{Sc}-like form (*PrP^{Sc}) when human neuroblastoma cells are exposed to an inorganic source of redox iron. The *PrP^{Sc} thus generated is itself redox active, and it induces the transformation of additional PrP^C, simulating *PrP^{Sc} propagation in the absence of brain-derived PrP^{Sc}. Moreover, limited depletion of iron from prion disease-affected human and mouse brain homogenates and scrapie-infected mouse neuroblastoma cells results in 4- to 10-fold reduction in proteinase K (PK)-resistant PrP^{Sc}, implicating redox iron in the generation, propagation, and stability of PK-resistant PrP^{Sc}. Furthermore, we demonstrate increased redox-active ferrous iron levels in prion disease-affected brains, suggesting that accumulation of PrP^{Sc} is modulated by the combined effect of imbalance in brain iron homeostasis and the redox-active nature of PrP^{Sc}. These data provide information on the mechanism of replication and toxicity by PrP^{Sc}, and they evoke predictable and therapeutically amenable ways of modulating PrP^{Sc} load.

INTRODUCTION

Prion disorders result from misfolding of the cellular prion protein (PrP^C) from a α-helical to a β-sheet–rich PrP-scrapie (PrP^{Sc}) isoform that is insoluble in nonionic detergents and partially resistant to digestion by proteinase K (PK). Accumulating evidence implicates PrP^{Sc} as the principal infectious and pathogenic agent in familial, infectious, and sporadic prion disorders (Prusiner, 1998; Aguzzi and Polymendiou, 2004). However, reports suggesting inconsistent correlation between PrP^{Sc} load, neuronal loss, and infectivity implicate other players besides PrP^{Sc} in prion disease-associated neurotoxicity (Lasmezas *et al*., 1997; Chiesa and Harris, 2001; Harris and True, 2006). One such player is the expression of PrP^C on neuronal plasma membrane. Absence of PrP^C renders neurons resistant to toxicity by PrP^{Sc}, whereas down-regulation of neuronal PrP^C expression reverses prion pathology in scrapie-infected mice (Mallucci *et al*., 2003; Chesebro *et al*., 2005). Whether PrP^C transmits the toxic signal directly or indirectly during conversion to PrP^{Sc} remains an open question. Recently, markers of oxidative stress and increased ferrous (Fe^{2+}) and ferric (Fe^{3+}) iron have been reported in the cerebral cortex, striatum, and brain stem of scrapie-infected mice and Creutzfeldt–Jakob disease (CJD)-affected human brains (Kim *et al*., 2000; Andreoletti *et al*., 2002; Hur *et al*., 2002; Fernaeus and Land, 2005). In some cases, PrP^{Sc} plaques colocalize with redox-active iron, suggesting a strong correlation between oxidative stress, PrP^{Sc} accumulation, and neuronal loss (Petersen *et al*., 2005). In addition, peroxidative damage has been linked directly to neuronal loss and de novo PrP^{Sc} propagation in scrapie-infected mice, establishing a causal link between oxidative damage, PrP^{Sc} propagation, and neurotoxicity (Brazier *et al*., 2006). Formation of redox-active copper complexes during PrP^C-to-PrP^{Sc} conversion (Thackray *et al*., 2002) and the presence of relatively stable PrP^{Sc}–ferritin complexes in sCJD brain tissue (Mishra *et al*., 2004) lend further support to the involvement of metal-induced oxidative stress in prion disease pathogenesis. The trigger leading to brain metal imbalance, however, remains unclear. In this report, we provide evidence that PrP^C is an iron-binding protein, a characteristic likely to modulate its susceptibility to oxidative damage. Using PrP^C-expressing neuroblastoma cells (PrP^C cells), we demonstrate that exposure to a source of redox iron such as inorganic ferrous chloride ($FeCl_2$) induces the conversion of PrP^C to a PrP^{Sc}-like form (*PrP^{Sc}) that resembles brain-derived PrP^{Sc} in several biochemical characteristics, including limited propagation in culture. More significantly, depletion of iron from prion disease-affected human and mouse brains and scrapie-infected mouse neuroblastoma (ScN2a) cells reduces

This article was published online ahead of print in *MBC in Press* (http://www.molbiolcell.org/cgi/doi/10.1091/mbc.E07–04–0317) on June 13, 2007.

[D] The online version of this article contains supplemental material at *MBC Online* (http://www.molbiolcell.org).

† These authors contributed equally to this work.

Address correspondence to: Neena Singh (neena.singh@case.edu).

Abbreviations used: CJDH, sCJD brain homogenate; DAB, 3,3′-diaminobenzidine; NH, normal brain homogenate; P_2I, high-speed detergent-insoluble pellet from mock and $FeCl_2$-exposed cells; P_2II, high-speed detergent-insoluble pellet from P_2I-exposed cells; ScH, scrapie-infected mouse brain homogenate.

PK-resistant PrP^{Sc} by 4- to 10-fold, suggesting that PrP^{Sc} generation, propagation, and stability are modulated by brain redox iron levels.

EXPERIMENTAL METHODS

Materials

Human neuroblastoma cells (M17) expressing PrP^{C} (PrP^{C} cells) were generated and maintained as described previously (Singh *et al*., 1997). Human astrocytoma cell line SW1088 (SW) was obtained from American Type Culture Collection (Manassas, VA) (HTB-12) and cultured in DMEM supplemented with 10% fetal bovine serum. Scrapie-infected mouse neuroblastoma cells (ScN2a) were obtained from Dr. Byron Caughey (Rocky Mountain Laboratories) and maintained as specified by Dr. Gregory Raymond (Rocky Mountain Laboratories). Mouse neuroblastoma cells (N2a) were obtained from American Type Culture Collection. Culture supplies were obtained from Invitrogen (Carlsbad, CA), and hygromycin B was obtained from Calbiochem (San Diego, CA). Recombinant PrP was a kind gift from Dr. Witold Surewicz (Case Western Reserve University). Primary antibodies 3F4 and 8H4 against PrP were purchased from Signet Laboratories (Dedham, MA) and provided by Drs. Pierluigi Gambetti and Man-Sun Sy (National Prion Surveillance Center, Case Western Reserve University), anti-ferritin antibody was from Sigma-Aldrich (St. Louis, MO), horseradish peroxidase (HRP)-labeled secondary antibodies were from GE Healthcare (Little Chalfont, Buckinghamshire, United Kingdom), fluorescein isothiocyanate- (FITC) and tetramethylrhodamine B isothiocyanate (TRITC)-labeled secondary antibodies were from Southern Biotechnology Associates (Birmingham, AL), and mouse and rabbit peroxidase-anti-peroxidase were from Cappel Laboratories (Cochranville, PA). LysoTracker and Hoechst were obtained from Invitrogen, and the silver staining kit was from Bio-Rad (Hercules, CA). EZ-Link sulfosuccinimidyl 2-(biotinamido)-ethyl-1,3-dithiopropionate (Sulfo-NHS-biotin) and Texas Red-conjugated streptavidin were from Pierce Chemical (Rockford, IL), and 3,3′-diaminobenzidine (DAB) was from Invitrogen. All other chemicals, including ferrous chloride, were obtained from Sigma-Aldrich.

Iron Labeling of Recombinant PrP

Recombinant PrP (5 μg in 20 μl of sodium acetate buffer, pH 4.0) was mixed with 10 μCi of $^{59}FeCl_3$, and the pH was adjusted to 7.4 with 1 ml of phosphate-buffered saline (PBS), pH 8.0. The reaction mixture was incubated at room temperature for 3 h, and then it was dialyzed against excess PBS for 72 h.

Native Gradient Gel Electrophoretic Separation

Linear 3–18% polyacrylamide gel was prepared using Hoefer SG gradient maker as described with minor modifications (Vyoral *et al*., 1998). The gel mixture contained 0.375 M Tris, pH 6.8, 1.5% Triton X-100, and 1.18 mM ammonium persulfate. *N*,*N*,*N*′,*N*′-Tetramethylethylenediamine was added to a final concentration of 5.38 mM for the 3% gel mixture and 2.69 mM for the 18% gel mixture. The prepared gel was left overnight at room temperature for polymerization. Radiolabeled PrP mixed with 5 μl of glycerol was subjected to electrophoresis under constant current for 3 h at 4°C. The gel was vacuum-dried and exposed to Kodak BioMax XAR film in Kodak X-Omatic cassette (Eastman Kodak, Rochester, NY) fitted with Lanex Regular intensifying screens for 72 h to 1 wk at −70°C.

$FeCl_2$ Treatment

In a typical experiment, 7×10^6 cells were exposed to 0.1, 0.2, or 0.3 mM $FeCl_2$ mixed in complete medium for 72 h (0.3 M stock in water). Subsequently, cells were washed three times with PBS and subcultured in 100-mm Petri dishes or on coverslips overnight in fresh medium lacking $FeCl_2$ before analysis.

Brain Tissue

Three cases each of normal (age 62–67 yr) and sCJD (age 60–67 yr), and five each of normal and scrapie-infected mouse brains were used for analysis. Human brain tissue was obtained from Dr. Gambetti, and mouse brain tissue was harvested from scrapie-infected mice (22L) generated in our facility. Brain homogenates (10%) were prepared in PBS or in lysis buffer and frozen in small aliquots until use.

Biotinylation

Cell lysates or brain homogenates were biotinylated with 1 mg/ml sulfo-NHS-biotin in PBS overnight at 4°C, and excess biotin was quenched with 50 mM glycine followed by desalting in a spin column. Small aliquots of biotinylated samples were frozen until use.

Differential Centrifugation

Cells were exposed to 10 μl of 10% NH or CJDH mixed in 5 ml of complete medium for 48 h or to desired concentrations of $FeCl_2$ for 72 h. Cells were then subjected to immunoprecipitation or differential centrifugation followed by Western blot analysis essentially as described previously (Singh *et al*., 1997).

Detection of Redox Iron

Modified Prussian blue reaction was used to detect redox-active ferrous and ferric iron in brain and cell lysate samples as described previously (Smith *et al*., 1997). Briefly, 5 μl of 10% mouse and human brain homogenate or P_2I fraction isolated from cells was dot blotted on a polyvinylidene difluoride (PVDF) membrane and allowed to dry at room temperature. Total protein concentration was 6.60 ± 0.09 and 4.73 ± 0.34 mg/ml in normal and sCJD samples, 10.71 ± 0.30 and 7.37 ± 0.22 mg/ml in normal and scrapie-infected mouse samples, and 6.78 ± 0.37 and 5.99 ± 0.14 mg/ml in -$FeCl_2$ P_2I and +$FeCl_2$ P_2I samples, respectively. Membranes were incubated overnight in 7% potassium ferrocyanide or potassium ferricyanide dissolved in 3% hydrochloric acid to detect ferric or ferrous iron, respectively. After the incubation, membranes were washed twice in distilled water for 5 min each and then incubated at room temperature with stable DAB containing 3% H_2O_2 until brown-blue color developed.

Determination of Total Iron

A colorimetric method was used to estimate total iron in brain and cell lysate samples according to the manufacturer's instructions (Teco Diagnostics, Anaheim, CA). Briefly, 200 μl of 10% brain homogenate or P_2I sample was dissolved in 1 ml of acetate buffer containing 220 mM hydroxylamine hydrochloride, pH 4.5, and 50 μl of 16.6 mM ferrozine. Change in color was recorded at 560 nm after 10 min of incubation at 37°C by using 500 mg/dl $FeCl_2$ solution as standard.

Treatment with Desferroxamine (DFO)

To chelate iron from brain homogenates, 10% homogenate of sCJD and mouse scrapie prepared in PBS was exposed to 100 μM DFO or vehicle for 10 min at room temperature, followed by extensive dialysis against PBS for 72 h. Subsequently, untreated and DFO-treated samples were supplemented with 10× lysis buffer before proteinase K digestion. For DFO exposure of ScN2a cells, semiconfluent (~70%) cultures were supplemented with 5 and 10 μM DFO or vehicle in serum-free medium for 24 h, washed in PBS, and harvested for PK treatment followed by Western blotting. (Surprisingly, DFO-treated cells looked healthier than vehicle-treated control cells at the end of 24 h.)

Immunostaining and Confocal Microscopy

Control and treated PrP^{C} cells were prepared for confocal microscopy as described in previous reports (Singh *et al*., 1997; Mishra *et al*., 2004).

RESULTS

Prion Disease-affected Human and Mouse Brains Show Increased Reactivity for Redox Iron

Because imbalance in iron homeostasis and markers of oxidative stress are a common feature of prion disease-affected brains and cultured cells (Kim *et al*., 2000; Wong *et al*., 2001; Fernaeus and Land, 2005), the amount of redox-active ferrous and ferric iron in mouse and human normal brain homogenate (NH), scrapie-infected mouse homogenate (ScH), and sporadic Creutzfeldt–Jakob disease-affected brain homogenate (CJDH) was estimated by reacting 5 μl of 10% brain homogenate spotted on a PVDF membrane with potassium ferri- and ferrocyanide, respectively, followed by incubation with DAB and H_2O_2 (modified Perl's reaction) (Smith *et al*., 1997). A brown reaction product with or without blue iron granules is indicative of a positive reaction. Remarkably, both ScH and CJDH samples show strong reactivity for ferrous and ferric iron compared with age-matched controls (Figure 1A). Quantification of total ferrozine-releasable iron shows four- to sixfold more iron in ScH and CJDH samples compared with age-matched controls (Figure 1B). To evaluate whether ferrous iron in CJDH is biologically active, 10 μl of biotin-tagged NH or CJDH (10% in PBS) was added to the culture medium of PrP^{C} cells. After 48 h, cell lysates were subjected to differential centrifugation followed by SDS-polyacrylamide gel electrophoresis (PAGE) and immunoblotting with anti-PrP antibody 3F4. Normally, PrP^{C} partitions almost exclusively in the detergent-soluble low- and high-speed supernatant fractions (S_1I, S_2I), whereas aggregated PrP^{Sc}-like forms are detected in the high-speed detergent-insoluble pellet fraction (P_2I). Nuclei and cell debris sediment in the low-speed pellet (P_1I) frac-

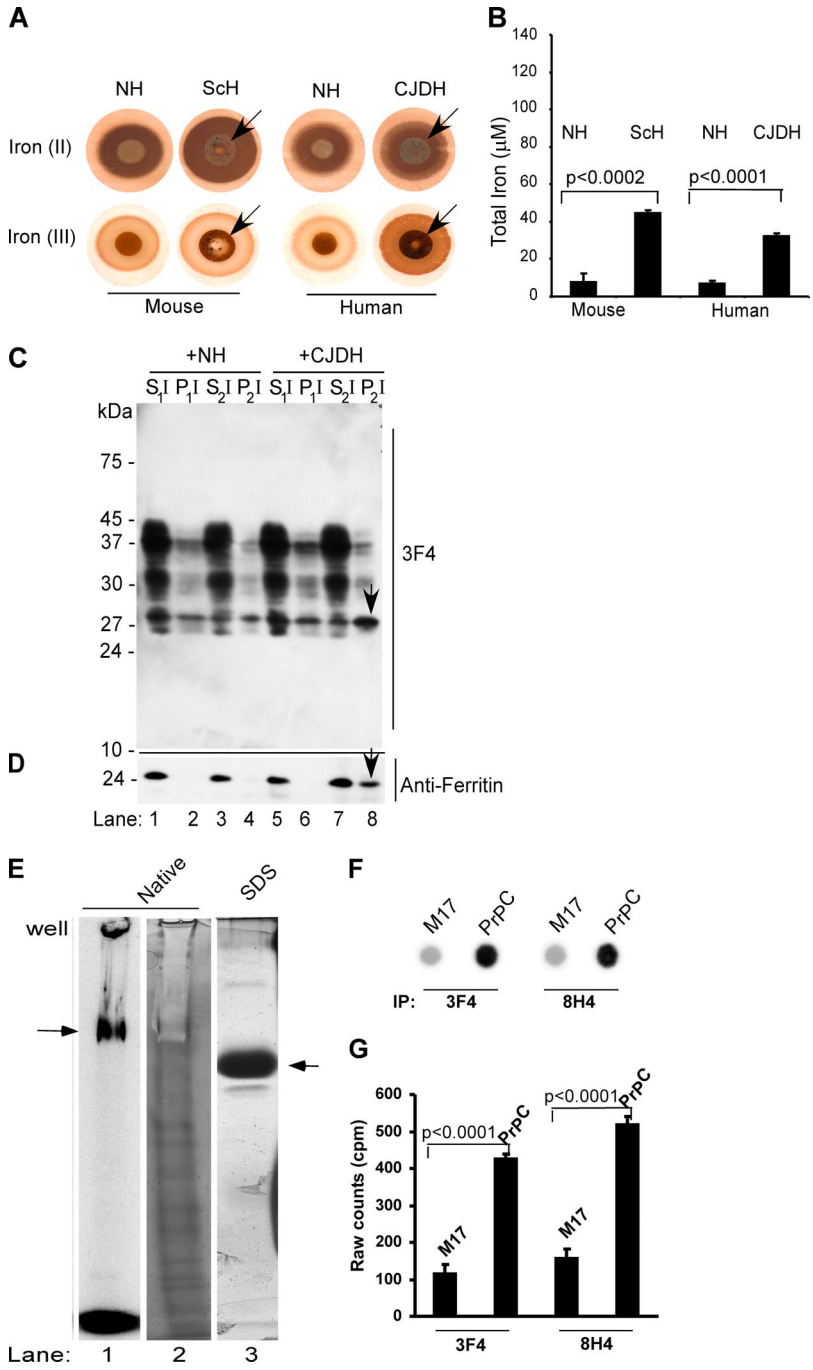

Figure 1. (A) Equal aliquots (5 μl each) of 10% brain homogenate from normal human and mouse (NH), scrapie-infected mouse (ScH), and sCJD were blotted on PVDF membrane and reacted for ferrous and ferric iron (Smith *et al.*, 1997). In contrast to NH, ScH and CJDH show strong reactivity for ferrous iron [Fe(II)]. Ferric iron is detected in all samples, but significantly more is in ScH and CJDH samples [Fe(III)]. (B) Colorimetric quantification of total iron shows four- to sixfold more iron in ScH and CJDH samples compared with age-matched NH controls. Unpaired *t* test shows highly significant mean difference between normal and diseased samples. Values for mouse samples: Δmean = 36.7; 95% confidence interval (CI) = 44.3, 29.2; $t = 13.5$; df = 8; $p < 0.0002$. Values for human samples: Δmean = 25.5; 95% CI = 29.2, 21.9; $t = 19.6$; df = 4; $p < 0.0001$). (C) Lysates of PrP^C cells exposed to biotin-tagged NH or CJDH were subjected to differential centrifugation and immunoblotted with 3F4. In NH-exposed lysates, most of PrP^C fractionates in the detergent-soluble S_1I and S_2I fractions (lanes 1 and 3). Minimal amounts of unglycosylated PrP^C are detected in the low- and high-speed detergent-insoluble fractions P_1I and P_2I (lanes 2 and 4). In contrast, CJDH-treated lysates show a significant amount of PrP in the high-speed detergent-insoluble P_2I fraction (lanes 5–8). (D) Reprobing with anti-ferritin shows slight up-regulation of ferritin in CJDH-treated lysates, 40% of which partitions in the P_2I fraction (lanes 1–8, arrow). (E) Recombinant PrP radiolabeled with $^{59}FeCl_3$–acetate complex shows a prominent iron-labeled band on native iron gel (lane 1) that shows a negative stain when stained with silver due to bound iron (lane 2). Minor bands that stain with silver probably represent degradation products that do not bind iron. Fractionation on SDS-PAGE and silver staining shows a single prominent band of recombinant PrP (lane 3). (F) M17 and PrP^C cells were radiolabeled with $^{59}FeCl_3$–citrate complex for 4 h and subjected to immunoprecipitation with 3F4 and 8H4. Eluted proteins were spotted on PVDF membrane followed by autoradiography. (G) Quantification of iron-labeled proteins in the immunoprecipitate by direct gamma-counting. n = 5. Unpaired *t* test shows highly significant mean difference between iron-labeled PrP immunoprecipitated from M17 and PrP^C cells. Values for 3F4 immunoprecipitates: Δmean = 313.1; 95% CI = 348.9, 277.3; $t = 24.3$; df = 8; $p < 0.0001$. Values for 8H4 immunoprecipitates: Δmean = 362.5; 95% CI = 404.2, 320.8; $t = 24.15$; df = 8; $p < 0.0001$.

tion. In the NH-treated sample, almost all of PrP^C fractionates in the detergent-soluble S_1I and S_2I fractions (Figure 1C, lanes 1–4). In contrast, a significant amount of PrP^C from CJDH-exposed lysates sediments in the detergent-insoluble P_2I fraction (Figure 1C, lanes 5–8). Reprobing with anti-ferritin shows slight up-regulation of ferritin and a prominent ferritin band in P_2I fraction of CJDH-exposed lysates (Figure 1D, lanes 1–8, arrow). Reaction of the same membrane with streptavidin shows no overlap of biotin-tagged proteins with PrP or ferritin (Supplemental Figure 1), confirming that aggregated PrP and ferritin in the P_2I fraction are from the cellular pool, not from added homogenate. Up-regulation of ferritin in CJDH-exposed PrP^C cells could be due to uptake of bioavailable ferrous iron from the sample, especially from the PrP^{Sc}–ferritin complex (Mishra *et al.*, 2004), or induction of stress due to other factors. Alternately, PrP^{Sc} itself could act as a source of iron, especially if PrP^C binds iron (Thompsett *et al.*, 2005). To investigate this possibility, recombinant PrP lacking His-tag (Morillas *et al.*, 1999) was radiolabeled with $^{59}FeCl_3$–acetate complex and fractionated on an iron gel essentially as described previously (Vyoral *et al.*, 1998). A prominent iron-labeled PrP band is noted in the native gel (Figure 1E, lane 1), demonstrating that purified PrP binds iron. Silver staining of the same sample evaluated in parallel reveals a negative stain for PrP due to bound iron, although minor bands that probably represent degradation products and do not bind iron show a positive stain with silver (Figure 1E, lane 2). Frac-

tionation of the same sample on SDS-PAGE that strips iron due to boiling in SDS shows a single prominent band by silver staining, confirming the purity of the sample (Figure 1E, lane 3). To check whether cell-associated PrP^C binds iron, nontransfected neuroblastoma cells (M17) and M17 cells transfected to express six- to eightfold more PrP^C (PrP^C cells) were incubated with $^{59}FeCl_3$–citrate complex for 4 h and processed for immunoprecipitation with 3F4 and 8H4. After stringent washing of beads, bound proteins were eluted with boiling SDS-sample buffer and counted directly in a gamma-counter. Subsequently, an aliquot of the same sample was dot-blotted on a PVDF membrane followed by autoradiography, and an equal amount was subjected to Western blotting to eliminate contamination with major iron-binding proteins such as ferritin and transferrin. As noted for recombinant PrP, cell-associated PrP^C shows significant incorporation of ^{59}Fe into PrP^C (Figure 1, F and G), and the signal is not derived from coimmunoprecipitated ferritin or transferrin (Supplemental Figure 2). Together, these data demonstrate increased levels of biologically active redox iron and a state of oxidative stress in prion disease-affected brains. In addition, PrP^C seems to bind iron, suggesting that the change in conformation of PrP^C to PrP^{Sc} with consequent sequestering of PrP^C-bound iron may account for brain iron imbalance. Because brain presents a complex milieu that is difficult to manipulate experimentally, further investigations aimed at understanding the role of redox iron in prion disease pathogenesis were carried out on PrP^C cells.

Exposure of PrP^C Cells to Redox Iron Induces the Accumulation of PrP

In a previous report, 0.3 mM inorganic ferrous chloride ($FeCl_2$) has been used successfully to induce oxidative damage to α-synuclein in a cell model (Ostrerova-Golts *et al.*, 2000). To identify the optimum concentration of $FeCl_2$ as close to the in vivo situation as possible, PrP^C cells were exposed to 0, 0.2, and 0.3 mM $FeCl_2$ in complete medium for 72 h, and cell lysates were compared with freshly harvested NH and ScH for cleavage of protein kinase C (PKC)δ into its catalytically active fragment as a positive marker of oxidative stress (Kaul *et al.*, 2003). Western blotting with anti-PKCδ antibody reveals full-length 74-kDa PKCδ protein in NH and in cells exposed to 0 and 0.2 mM $FeCl_2$ (Supplemental Figure 3, A and B). In contrast, ScH and lysates from cells exposed to 0.3 mM $FeCl_2$ show the catalytically active 41-kDa fragment of PKCδ, indicating that 0.3 mM $FeCl_2$ simulates the in vivo conditions of oxidative stress within the limitations of this method. An additional fragment of 25 kDa of unknown significance is also noted in ScH and 0.3 mM $FeCl_2$-exposed samples (Supplemental Figure 3B). Reprobing of cell lysates with 3F4 shows the expected glycoforms of PrP^C migrating at 27, 28–30, and 37 kDa in untreated lysates (Figure 2A, lane 1). Exposure to $FeCl_2$ causes significant up-regulation of PrP^C, and additional bands of 20 and 12 kDa show up when the concentration is increased from 0.2 to 0.3 mM (Figure 2A, lanes 2 and 3). (The apparently greater up-regulation of PrP^C by 0.2 mM $FeCl_2$ compared with the higher dose is because of PrP^C aggregation by 0.3 mM $FeCl_2$; Supplemental Figure 4 and Figures 2C and 3A) Reprobing for ferritin shows greater than 10-fold up-regulation and partial cleavage of ferritin, resulting in a 14-kDa fragment on exposure to $FeCl_2$ (Figure 2B, lanes 2 and 3). The difference in PrP^C and ferritin levels is not due to differential loading as determined by silver staining of the membrane after immunoblotting (data not shown). Morphological evaluation of PrP^C cells exposed to vehicle or 0.3 mM $FeCl_2$ was carried out by immunoreacting permeabilized cells with 3F4, 8H4, or anti-ferritin followed by appropriate peroxidase-conjugated secondary antibodies and reaction with DAB. Vehicle-treated cells show normal distribution of PrP^C on the plasma membrane and in the Golgi area with both 3F4 and 8H4 (Figure 2C, 1 and 3). In contrast, cells exposed to $FeCl_2$ show barely detectable immunoreactivity with 3F4 (Figure 2C2) and strong intracellular reaction with 8H4 (Figure 2C4). Similar evaluation with anti-ferritin shows strong intracellular reaction in $FeCl_2$-exposed cells compared with vehicle-treated controls (Figure 2C, 5 and 6), whereas nuclear morphology remains unaltered (Figure 2C, 1–6).

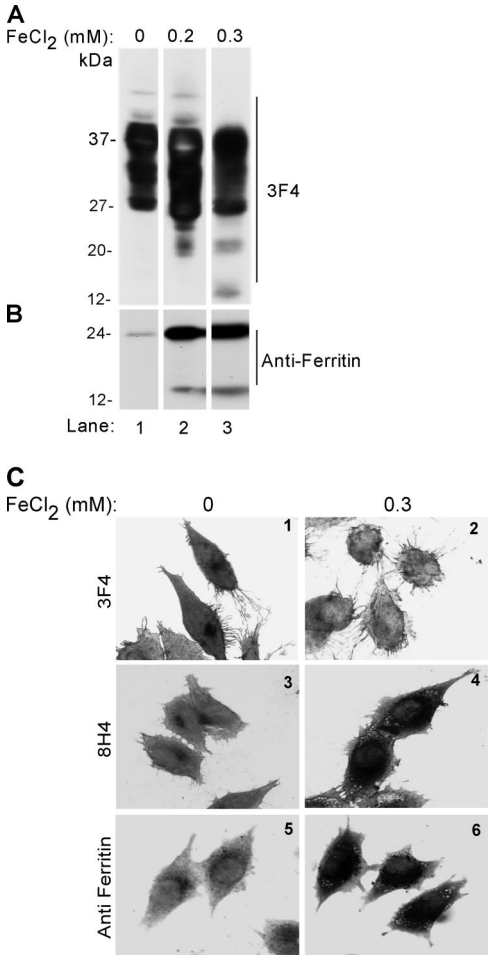

Figure 2. (A) Immunoblotting of mock-treated lysates with 3F4 shows the expected glycoforms of PrP^C (lane 1). After exposure to 0.2 or 0.3 mM $FeCl_2$, additional bands of 26, 20, and 12 kDa are detected (lanes 2 and 3). (B) Reprobing for ferritin shows a significant increase in ferritin signal by exposure to 0.2 and 0.3 mM $FeCl_2$, and appearance of a 14-kDa cleavage product. (C) Mock and 0.3 mM $FeCl_2$-treated PrP^C cells were permeabilized and immunoreacted with 3F4, 8H4, or anti-ferritin antibodies. After incubation with appropriate peroxidase-conjugated secondary antibodies, the cells were reacted with DAB and observed. Mock-treated cells show PrP reaction in the Golgi region with both 3F4 and 8H4 antibodies (1 and 3). In contrast, $FeCl_2$-treated cells do not react with 3F4, but they show a strong reaction with 8H4 (panels 2 and 4). Strong reactivity for ferritin is observed in $FeCl_2$ exposed cells in comparison to mock-treated controls (5 and 6).

Cellular PrP^C Is Converted to a PrP^{Sc}-like Form ($*PrP^{Sc}$) by $FeCl_2$

Insolubility in nonionic detergents and limited resistance to digestion by proteinase K are hallmarks of PrP^{Sc} isolated from diseased brains. To evaluate whether $FeCl_2$-induced PrP^C possesses any of the biophysical characteristics of PrP^{Sc}, lysates of PrP^C cells exposed to $FeCl_2$ for 72 h were fractionated as described in Figure 1C. As expected, PrP^C from mock-treated lysates partitions almost exclusively in the detergent-soluble S_1I and S_2I fractions (Figure 3A, lanes 1–4). In contrast, PrP^C from $FeCl_2$-exposed cells partitions in the low-speed pellet P_1I and high-speed pellet P_2I fractions (Figure 3A, lanes 5–8). Reprobing with anti-ferritin reveals 8- to 10-fold up-regulation of ferritin in treated cells, 40% of which partitions in the P_2I fraction (Figure 3B, lanes 1–8). Quantification reveals an increase in detergent-insoluble PrP from 28 to 55% after exposure to $FeCl_2$ (Supplemental Figure 4). Reprobing with anti-β-actin shows no effect of $FeCl_2$ on β-actin expression or detergent solubility, and equivalent protein loading in all lanes (Figure 3C, lanes 1–8). Sensitivity to PK was estimated by treating mock- and $FeCl_2$-exposed lysates to 0, 7.5, and 15 μg/ml PK for 5 min at 37°C. The reaction was stopped with 4 mM phenylmethylsulfonyl fluoride, and PK-resistant PrP was visualized by immunoblotting with 3F4. Mock-treated lysates show the expected glycoforms of PrP^C, all of which are digested by 7.5 μg/ml PK (Figure 3D, lanes 1–3). In contrast, $FeCl_2$-treated lysates show limited resistance of PrP to PK and the generation of a 20-kDa C-terminal fragment (Figure 3D, lanes 4–6). Reprobing with anti-ferritin reveals up-regulation of ferritin and resistance to digestion with 7.5 and 15 μg/ml PK, although a minor fraction is cleaved and releases a fragment of ~14 kDa (Figure 3E, lanes 1–6). To evaluate whether change in conformation of PrP^C to a PrP^{Sc}-like form ($*PrP^{Sc}$) as evidenced by detergent insolubility and PK resistance is a direct effect of redox iron, a similar evaluation was carried out on human astrocytoma cell line (SW) that expresses ceruloplasmin on the plasma membrane, a protein known to shuttle excess iron and copper ions out of the cell (Patel and David, 1997). Differential centrifugation of mock- and $FeCl_2$-exposed SW cells does not reveal aggregation or up-regulation of PrP^C or ferritin, confirming a direct role of redox iron in this process (Supplemental Figure 5, A and B, lanes 1–8). Together, the above-mentioned data demonstrate that exposure of neuroblastoma cells to redox iron causes a change in conformation of PrP^C to $*PrP^{Sc}$. Astrocytes provide a protective environment for PrP^C under these circumstances due to their inherent capacity to shuttle excess iron out of the cells, a property lacking in neuroblastoma cells.

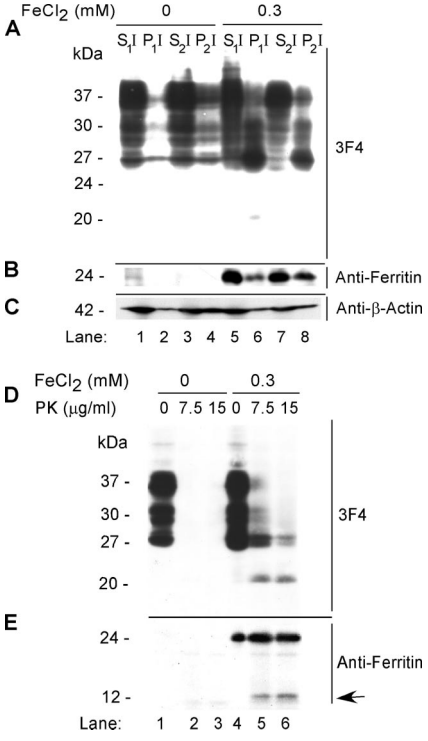

Figure 3. (A) Mock- and 0.3 mM $FeCl_2$-exposed cell lysates were fractionated by differential centrifugation and immunoblotted with 3F4. As expected, the majority of PrP^C from mock-treated lysates partitions in the detergent-soluble S_1I and S_2I fractions (lanes 1 and 3), with minimal amounts in the P_1I and P_2I fractions (lanes 2 and 4). In contrast, significant amounts of PrP^C from $FeCl_2$-treated lysates are detected in the pellet fractions P_1I and P_2I (lanes 6 and 8). A minor 20-kDa fragment is observed in the P_1I fraction of treated cells (lane 6). (B) Reprobing with anti-ferritin shows up-regulation of ferritin in $FeCl_2$-treated lysates (lanes 1–8), 40% of which partitions in the P_2I fraction (lane 8). (C) $FeCl_2$ treatment has no detectable effect on the expression or solubility of β-actin. (D) Treatment of lysates prepared from mock- and $FeCl_2$-exposed cells with 7.5 and 15 μg/ml PK results in the complete digestion of PrP^C in mock-treated controls (lanes 1–3), whereas treated lysates show a 20-kDa PK-resistant fragment (lanes 4–6). (E) Reprobing with anti-ferritin shows up-regulation of ferritin in $FeCl_2$-exposed cells (lanes 1–6) and the generation of a 14-kDa fragment by PK (lanes 5 and 6, arrow).

Ferrous Iron-induced $*PrP^{Sc}$ Is Associated with Ferritin

In a previous study, we reported that PrP^{Sc} and ferritin form a complex in brain homogenates of sCJD cases (Mishra *et al*., 2004). To identify the presence of a similar complex in our model, mock- and $FeCl_2$-exposed cells were coimmunostained with 8H4-anti-mouse FITC and anti-ferritin-anti-rabbit TRITC. (To eliminate autofluorescence, cells were washed and cultured overnight in medium lacking $FeCl_2$.) In mock-treated cells, distinct PrP^C and ferritin reaction is detected in the Golgi area and cytosol, respectively (Figure 4A, 1–3). In $FeCl_2$-treated cells, in contrast, PrP and ferritin reaction is severalfold higher, and both proteins colocalize in intracellular vesicular structures (Figure 4A, 4–6, arrows). Reaction of $FeCl_2$-exposed cells with the lysosome-specific dye LysoTracker and 8H4-anti-mouse FITC shows localization of PrP within lysosomes (Figure 4B, 1–3, arrows). To evaluate whether PrP and ferritin are associated with each other within lysosomes, PrP^C cells exposed to 0, 0.2, or 0.3 mM $FeCl_2$ for 72 h were lysed in nondenaturing buffer and immunoprecipitated with 8H4 or anti-ferritin antibodies. Eluted proteins were fractionated by SDS-PAGE and immunoblotted with 3F4. In 8H4 immunoprecipitates, as expected, normal glycoforms of PrP^C are detected. It is notable that the intensity of all PrP^C glycoforms increases after $FeCl_2$ exposure as noted in Figure 2A (Supplemental Figure 6, lanes 1–3). Surprisingly, anti-ferritin immunoprecipitates of treated lysates pull down all three glycoforms of PrP^C, especially the unglycosylated form that almost doubles in intensity when $FeCl_2$ is increased from 0.2 to 0.3 mM (Supplemental Figure 6, lanes 5 and 6, arrowhead). A small amount of PrP^C from untreated lysates also coimmunoprecipitates with anti-ferritin, a reproducible finding that is currently under investigation (Supplemental Figure 6, lane 4). Control immunoprecipitates in the absence of antibodies do not reveal any detectable bands with 8H4 or anti-ferritin, ruling out nonspecific binding to protein A beads (Supplemental Figure 6, lanes 7–9). The difference in PrP signal in

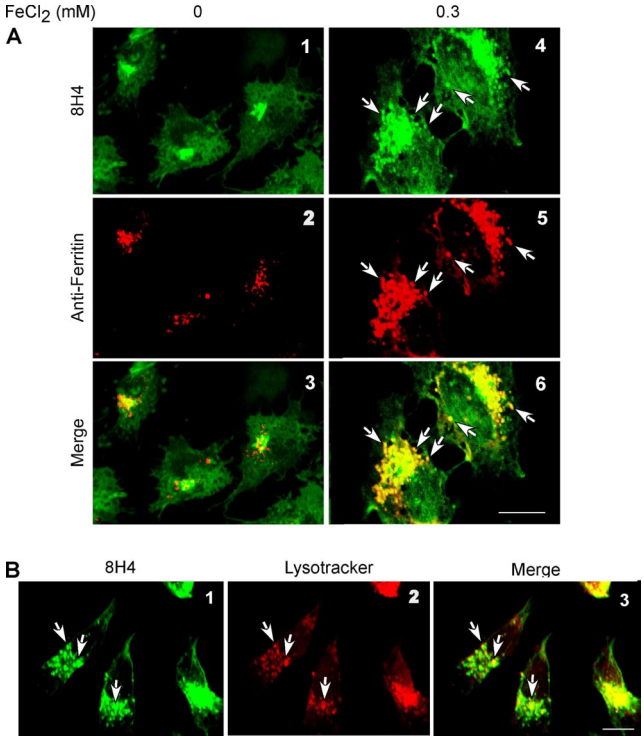

Figure 4. (A) Mock and 0.3 mM $FeCl_2$-treated PrP^C cells were permeabilized and immunoreacted with 8H4-anti-mouse FITC and anti-ferritin-anti-rabbit TRITC antibodies. In mock-treated cells, PrP^C reaction is detected in the Golgi area, and it does not overlap with ferritin reactivity (1–3). In $FeCl_2$-exposed cells, PrP and ferritin reactivity is severalfold higher, and PrP reaction colocalizes with ferritin (4–6). (B) Immunostaining of $FeCl_2$-exposed cells with 8H4-anti-mouse FITC and lysosome-specific dye LysoTracker shows localization of PrP within lysosomes (1–3).

lanes 2 and 3 is due to aggregation of PrP^C and coimmunoprecipitation with anti-ferritin when exposed to 0.3 mM $FeCl_2$ (Supplemental Figure 4). Thus, $*PrP^{Sc}$ and ferritin form a coimmunoprecipitable complex in $FeCl_2$-exposed cells.

Ferrous Chloride-induced $*PrP^{Sc}$–Ferritin Complex Propagates $*PrP^{Sc}$ Conformation

Brain-derived PrP^{Sc} has the unique capability of inducing a similar change in neighboring PrP^C, resulting in PrP^{Sc} replication. To evaluate whether $*PrP^{Sc}$ induced by $FeCl_2$ can induce the aggregation of additional PrP^C, lysates of mock-treated ($-FeCl_2$) and $FeCl_2$-exposed ($+FeCl_2$) cells were biotinylated, subjected to differential centrifugation, and the P_2I fraction was resuspended in 400 μl of PBS. Subsequently, 5 μl of biotin-tagged -$FeCl_2$ P_2I and $+FeCl_2$ P_2I was added to the culture medium of PrP^C cells for 72 h, and lysates were fractionated by differential centrifugation as described above. (For clarity, protein fractions obtained from cells exposed to P_2I are identified with the roman II.) Immunoblotting with 3F4 shows almost all PrP in the detergent-soluble S_1II and S_2II fractions of $-FeCl_2$ P_2I-exposed cells, as in Figure 3A (Figure 5A, lanes 1–4). In contrast, exposure to $+FeCl_2$ P_2I results in a significant shift of PrP to the detergent-insoluble P_1II and P_2II fractions (Figure 5A, lanes 6 and 8). Reprobing with anti-ferritin shows 8- to 10-fold up-regulation of ferritin in cells exposed to $+FeCl_2$ P_2I, 60% of which is detected in the P_2II fraction (Figure 5B, lanes 5–8). Reprobing with anti-β-actin shows no alteration of β-actin levels in $-FeCl_2$ P_2I- and $+FeCl_2$ P_2I-exposed cell lysates (Figure 5C, lanes 1–8). Reaction with streptavidin-HRP shows that added biotin-tagged $+FeCl_2$ P_2I is endocytosed by PrP^C cells and sediments in the P_1II fraction (Figure 5D, lane 6). It is notable that biotin-tagged material is absent from $-FeCl_2$ P_2I-exposed cells, suggesting that either $-FeCl_2$ P_2I is not internalized at all, or is degraded after endocytosis. The detergent-insoluble PrP in the P_2II fraction of $+FeCl_2$ P_2I-exposed cells, therefore, represents newly aggregated $*PrP^{Sc}$ induced by the treatment. Next, sensitivity of lysates prepared from cells exposed to 0.3 mM $FeCl_2$, $+FeCl_2$ P_2I, and $-FeCl_2$ P_2I to limited digestion with PK was assessed. After treatment with 0, 7.5, and 15 μg/ml PK for 5 min at 37°C, PK-resistant PrP was detected by immunoblotting with 3F4. Remarkably, both 0.3 mM $FeCl_2$ and $+FeCl_2$ P_2I result in the generation of a 20-kDa C-terminal PK-resistant fragment typical of disease-associated PrP^{Sc} (Figure 5E, lanes 4–6 and 10–12), whereas PrP from mock-treated and $-FeCl_2$ P_2I-exposed cells is completely degraded (Figure 5E, lanes 1–3 and 7–9). A comparison of protein fractions isolated from $-FeCl_2$ P_2I- and $+FeCl_2$ P_2I-exposed lysates shows up-regulation of proteins in the 100- and 10- to 35-kDa range in the $+FeCl_2$ P_2II fraction (Supplemental Figure 7). Total iron content of the two fractions is 0.008 and 0.12 mM, respectively (Supplemental Figure 8B). However, exposure of PrP^C cells to 0.1 and 0.2 mM $FeCl_2$ for 72 h does not result in the aggregation or PK resistance of PrP^C (Figure 5, F and G), indicating that $+FeCl_2$ P_2I-induced aggregation and PK resistance of additional PrP^C is not simply due to the iron content of this fraction. Cellular localization and physical proximity of PrP aggregates to $+FeCl_2$ P_2I was evaluated by immunostaining permeabilized cells with streptavidin-Texas Red to identify added P_2I and 8H4-FITC to visualize endogenous PrP. All cells show variable sizes of streptavidin-reactive P_2I aggregates on the cell surface and in endocytic vesicles (Figure 5H, 1–3). Higher magnification image of two cells from images 1 to 3 shows P_2I-induced coaggregation of endogenous PrP (Figure 5H, 4–6), whereas other cells show distinct reaction for P_2I and PrP with limited or no colocalization (Figure 5H, 7–9). Most treated cells show increased immunoreaction for PrP, indicating $+FeCl_2$ P_2I-induced up-regulation as noted for $FeCl_2$-treated cells (Figure 5H, 1–9). Coimmunostaining with anti-ferritin and anti-PrP antibodies shows partial colocalization of the two proteins as observed in Figure 4A (Figure 5H, 10–12). To evaluate whether the above-mentioned results are due to the redox-active nature of $+FeCl_2$ P_2I, ferrous and ferric iron content of 5 μl of $-FeCl_2$ P_2I and $+FeCl_2$ P_2I was analyzed as described in Figure 1A. In comparison with $-FeCl_2$ P_2I, the $+FeCl_2$ P_2I sample shows significantly higher ferrous and ferric iron reactivity (Supplemental Figure 8A). Quantitative analysis of the total iron pool shows 12-fold more iron in $+FeCl_2$ P_2I compared with $-FeCl_2$ P_2I sample (Supplemental Figure 8B), and 3–4 times more iron than ScH and sCJDH, respectively (compare with Figure 1B). Together, the above-mentioned results demonstrate that exposure of PrP^C cells to redox iron results in the up-regulation of PrP^C and ferritin and that PrP^C undergoes a change in conformation to $*PrP^{Sc}$ that coaggregates with ferritin within lysosomes. More importantly, aggregated PrP–ferritin complex can seed the aggregation of additional PrP^C when added to fresh cells, simulating $*PrP^{Sc}$ propagation in the absence of infectious brain homogenate.

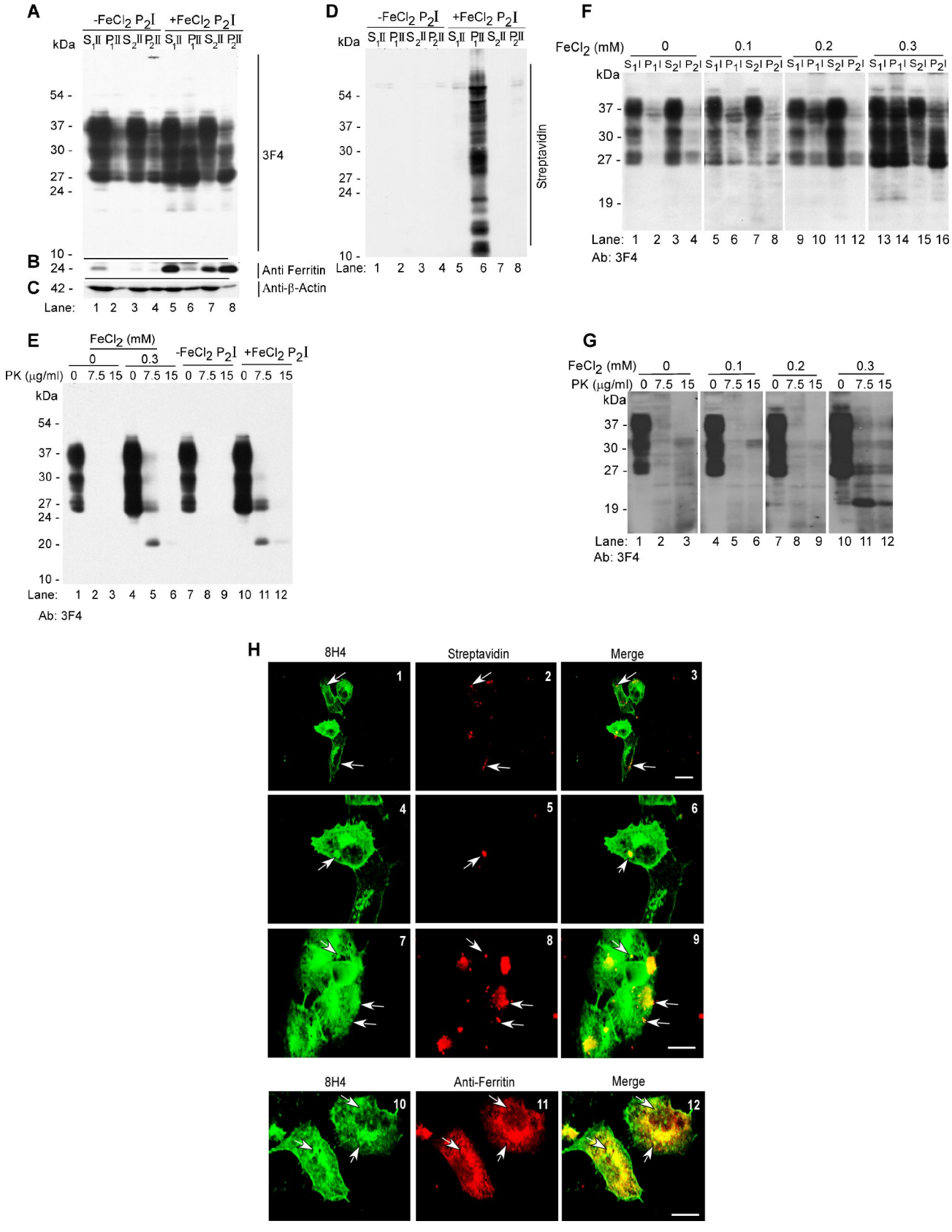

Figure 5. (A) Lysates of $-FeCl_2$ P_2I- or $+FeCl_2$ P_2I-treated PrP^C cells were subjected to differential centrifugation and immunoblotted with 3F4. The majority of PrP^C from $-FeCl_2$ P_2I samples fractionates in the detergent-soluble S_1II and S_2II fractions (lanes 1–4). In contrast, a significant proportion of PrP^C from $+FeCl_2$ P_2I lysates shifts to the detergent-insoluble P_1II and P_2II fractions (lanes 5–8). (B) Reprobing with anti-ferritin shows up-regulation and shift to P_2II fraction of a significant amount of ferritin in the $+FeCl_2$ P_2I-exposed sample (lanes 1–8).

Depletion of Iron Reduces PK-resistant PrP^{Sc} in Diseased Tissue and Infected Cells

To evaluate the influence of iron on infectious PrP^{Sc}, sCJD- and scrapie-infected mouse brain homogenates prepared in PBS were treated with vehicle or 100 μM DFO for 5 min at room temperature, and the samples were dialyzed extensively against PBS for 72 h. Recovered sCJD samples were subjected to another round of DFO treatment and dialysis, whereas mouse brain samples were analyzed as such. After dialysis, an aliquot of each was spotted on a PVDF membrane to assess ferrous and ferric iron content in untreated and DFO-treated samples (Figure 6, D and H), and an additional aliquot was supplemented with detergent, exposed to PK, and analyzed by Western blotting. Immunoblotting of control and DFO-treated sCJD homogenate with 3F4 shows the expected glycoforms of PrP migrating between 27 and 40 kDa (Figure 6A, lanes 1 and 2). Treatment with 100 μg/ml PK for 1 h at 37°C results in the generation of C-terminal PK-resistant fragments of PrP^{Sc} in the untreated control, whereas DFO-treated sample shows almost complete absence of PK-resistant PrP^{Sc} (Figure 6A, lanes 3 and 4, white arrow). Reprobing for ferritin shows no apparent difference between control and DFO-treated samples (Figure 6B, lanes 1 and 2), although PK treatment of DFO-treated sample causes slight decrease in monomeric ferritin migrating at 20 kDa and disappearance of some oligomeric forms (Figure 6B, lanes 3 and 4, arrowhead). Silver staining of PK-treated samples confirms that the difference in PrP and ferritin reactivity noted above is not an artifact of loading (Figure 6C, lanes 3 and 4). (The membranes were not probed for β-actin because PK cleaves this protein (data not shown). Reaction of control and DFO-treated samples for ferrous and ferric iron shows significant reduction of both forms, especially ferric iron after DFO treatment (Figure 6D). Quantification from four independent evaluations shows a decrease in PK-resistant PrP^{Sc} and ferritin from 99 to 10% and from 100 to 80%, respectively, after DFO treatment (Figure 6E). Similar evaluation of scrapie-infected mouse brain homogenate shows a significant decrease in PK-resistant PrP^{Sc} after DFO treatment (Figure 6F, lanes 1–4, white arrow). Reprobing for ferritin shows, surprisingly, generation of monomeric ferritin by merely DFO treatment (Figure 6G, lane 2, black arrow). Exposure to PK results in degradation of monomeric ferritin regardless of DFO treatment (Figure 6G, lanes 3 and 4), and disappearance of a minor band after DFO exposure (Figure 6G, lanes 2 and 4, arrowhead). Quantification from four independent experiments shows a decrease in PK-resistant PrP^{Sc} from 98 to 25% and no significant change in ferritin, regardless of DFO treatment (Figure 6I). The relatively less effect of DFO on PK sensitivity of mouse PrP^{Sc} compared with sCJD is perhaps due to reduced chelation of iron from these samples (Figure 6, H vs. D). The differential PK sensitivity of ferritin monomers and oligomers from human and mouse brains is unclear from our data. To determine whether depletion of iron has similar effect on ScN2a cells that actively replicate and accumulate infectious PrP^{Sc} in culture, cells were exposed to vehicle or 5 and 10 μM DFO in serum-less medium for 24 h and harvested in a buffer containing nonionic detergents. Lysates containing equivalent protein were treated with 7.5 and 15 μg/ml PK for 5 min at 37°C, and methanol-precipitated proteins were fractionated by SDS-PAGE and transferred to PVDF membrane. To ensure equal loading, transferred proteins were visualized by staining with Ponsue Red (Supplemental Figure 9) followed by immunoblotting with 8H4 and anti-ferritin. Probing with β-actin was omitted, because PK cleaves this protein. Reaction with 8H4 shows the expected glycoforms of PrP that are relatively resistant to digestion by 7.5 and 15 μg/ml PK, although some sensitivity is observed at the higher dose (Figure 7A, lanes 1–3). (This is expected because PrP^{Sc} from this cell line is cleaved by 20 μg/ml PK for 60 min at 37°C; Taraboulos *et al*., 1990.) Similar evaluation of lysates prepared from DFO-treated cells shows a dose-dependent decrease in PK-resistant PrP^{Sc} (Figure 7A, lanes 4–9). Reprobing for ferritin shows slight PK sensitivity of oligomeric and monomeric ferritin regardless of DFO treatment (Figure 7B, lanes 1–9). Some forms decrease in intensity (Figure 7B, lanes 1–9, black arrows), whereas others increase as higher order oligomers are reduced to lower order complexes (lanes 1–9, white arrowhead). Quantification from four independent experiments shows a significant decline in PK-resistant PrP^{Sc} from 99 to 70% and from 70 to 40% with 7.5 and 15 μg/ml PK, respectively, after exposure to 5 μM DFO. A further decline of PK-resistant PrP^{Sc} to 30 and 18% is observed when the DFO concentration is increased to 10 μM (Figure 7C). Similar quantification of ferritin shows 75–95% PK-resistant ferritin regardless of DFO treatment (Figure 7D). To rule out possible cytotoxicity by DFO, viability of N2a and ScN2a cells exposed to 10 μM DFO or vehicle for 24 h was quantified by terminal deoxynucleotidyl transferase dUTP nick-end labeling (TUNEL) staining. Twenty random 20× microscopic fields were examined, and the percentage of TUNNEL-positive cells was calculated. Based on these results, DFO-treated N2a cells show a slight increase in cell death in comparison with untreated controls from 5 to 8%, whereas similarly treated ScN2a cells show a reduction in cell death from 10 to 5%, respectively (data not shown). Surprisingly, iron chelation seems to improve the viability of ScN2a cells. Thus, depletion of iron from infectious brain homogenates or scrapie-infected cells reduces the total amount of PK-resistant PrP^{Sc} to a significant extent. Notably, ferritin does not show a

Figure 5 (cont). (C) Cellular β-actin levels remain unchanged under these conditions (lanes 1–8). (D) Reaction of the same membrane with streptavidin-HRP shows biotin-tagged proteins only in the P_1II fraction of $+FeCl_2$ P_2I-exposed sample (lane 6). (E) Treatment of mock-, 0.3 mM $FeCl_2$-, $-FeCl_2$ P_2I-, or $+FeCl_2$ P_2I-treated lysates with 7.5 and 15 μg/ml PK shows complete digestion of PrP^C in mock- and -$FeCl_2$ P_2I-exposed samples (lanes 1–3 and 7–9). In contrast, 0.3 mM $FeCl_2$- and $+FeCl_2$ P_2I-exposed samples show partial resistance to 7.5 μg/ml PK, resulting in the generation of a 20-kDa fragment (lanes 4–6 and 10–12). (F) Lysates of PrP^C cells exposed to 0, 0.1, 0.2, and 0.3 mM $FeCl_2$ for 72 h were subjected to differential centrifugation and immunoblotting with 3F4. The majority of PrP^C from cells exposed to 0, 0.1, and 0.2 mM $FeCl_2$ fractionates in the detergent-soluble S_1I and S_2I fractions (lanes 1–12). In contrast, a significant proportion of PrP^C from cells exposed to 0.3 mM $FeCl_2$ shifts to the detergent-insoluble P_1I and P_2I fractions (lanes 13–16). (G) Treatment of lysates from F above with 7.5 and 15 μg/ml PK shows complete digestion of PrP^C from samples exposed to 0, 0.1, and 0.2 mM $FeCl_2$ (lanes 1–9). In contrast, the sample exposed to 0.3 mM $FeCl_2$ shows partial resistance to 7.5 and 15 μg/ml PK, resulting in the generation of 20-kDa C-terminal fragment (lanes 10–12). (H) PrP^C cells exposed to biotin-tagged $+FeCl_2$ P_2I were permeabilized and reacted with 8H4-anti-mouse FITC and streptavidin-Texas Red. Streptavidin-positive aggregates are detected on the plasma membrane and in endocytic vesicles (1–3). Higher magnification of select cells from 1 to 3 shows aggregation of PrP around streptavidin-positive aggregates in some areas (4–6) and distinct PrP and streptavidin reaction in other regions (7–9). All cells show upregulation of PrP (1–9). Coimmunostaining with 8H4-anti-mouse FITC and anti-ferritin-anti-rabbit TRITC shows colocalization of the two proteins in vesicular structures near the Golgi region (10–12).

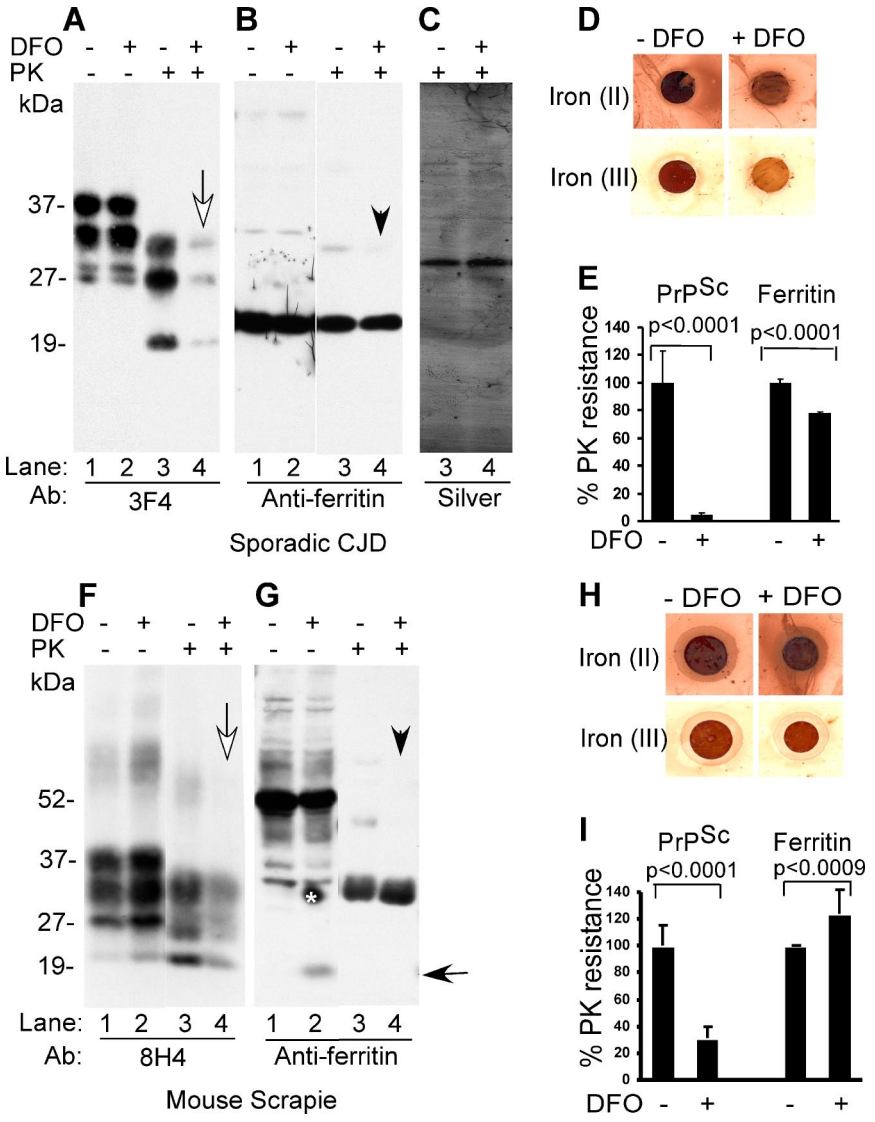

Figure 6. (A) Control and DFO-treated sCJD homogenate and the same samples treated with PK were fractionated on SDS-PAGE and analyzed by Western blotting. Immunoblotting with 3F4 reveals normal PrP glycoforms in control and DFO-treated samples (lanes 1 and 2). Treatment with PK causes the expected shift in migration of PK-resistant PrP^{Sc} in the control sample (lane 3), whereas DFO-treated sample shows almost complete degradation of PrP^{Sc} (lane 4, white arrow). (B) Reprobing with anti-ferritin shows similar monomeric and oligomeric forms of ferritin in control and DFO-treated samples (lanes 1 and 2). However, DFO-treated samples show slight increase in sensitivity to PK, especially of oligomeric forms (lanes 3 and 4, arrowhead). (C) Silver staining shows equal amount of protein in PK-treated control and DFO-treated samples (lanes 3 and 4). (D) Reaction for ferrous and ferric iron in sCJD samples shows significant reduction in especially the ferric form after DFO treatment. (E) Quantification from four independent evaluations shows a decrease in PK-resistant PrP^{Sc} and ferritin from 99 to 10% and from 100 to 80%, respectively, after DFO treatment. n = 4. Unpaired *t* test shows highly significant mean difference between PK-resistant PrP and ferritin in untreated and DFO-treated CJDH. Values for PK-resistant PrP: Δmean = 95.2; 95% CI = 78.8, 111.6; t = 12.3; df = 6; $p < 0.0001$. Values for PK-resistant ferritin: Δmean = 21.6; 95% CI = 419.5, 23.7; t = 22.0; df = 6; $p < 0.0001$. (F) Immunoblotting of mouse scrapie brain homogenate with 8H4 shows the expected glycoforms of PrP^{Sc} in control and DFO-treated samples (lanes 1 and 2). After PK treatment, a significant amount of PrP^{Sc} from DFO-treated samples undergoes degradation (lanes 3 and 4). (G) Reprobing for ferritin shows prominent oligomers of ferritin migrating between 35 and 55 kDa (lanes 1 and 2), some of which are sensitive to DFO and give rise to monomeric ferritin migrating at 20 kDa (lane 2, black arrow). Treatment with PK shows increased sensitivity of monomeric and DFO-treated oligomeric forms of ferritin (lanes 3 and 4, arrowhead) (*, artifact of blotting). (H) Reaction of mouse brain homogenate for ferrous and ferric iron shows significantly less reactivity after DFO treatment. (I) Quantification shows a decrease in PK-resistant PrP^{Sc} from 98 to 25% after DFO treatment. Ferritin does not show a significant difference before or after DFO treatment. n = 4. Unpaired *t* test shows highly significant mean difference between PK-resistant PrP, and less significant difference between PK-resistant ferritin in untreated and DFO-treated mouse scrapie samples. Values for PK-resistant PrP: Δmean = 69.2; 95% CI = 56.4, 82.0; t = 11.4; df = 6; $p < 0.0001$. Values for PK-resistant ferritin: Δmean = 24.0; 95% CI = 36.6, 11.5; t = 4.0; df = 6; $p < 0.0009$.

proportional decline in PK resistance, indicating distinct response of these proteins to iron depletion.

DISCUSSION

We demonstrate that exposure of PrP^{C} cells to a source of redox iron results in the generation of $*PrP^{Sc}$, a PrP^{Sc}-like molecule that induces a similar change in additional PrP^{C} when added to fresh cells. More importantly, depletion of iron from human and mouse infectious brain homogenates reduces the amount of PK-resistant PrP^{Sc}, implicating redox iron in the generation, propagation, and stability of PK-resistant PrP^{Sc}. Although a change in conformation of recombinant and purified PrP^{C} to a PrP^{Sc}-like molecule has been reported by other groups by using a variety of in vitro reaction conditions (see below), this is the first demonstration where generation and propagation of a PrP^{Sc}-like molecule has been achieved by an inorganic trigger in cells, a model that is biologically relevant and provides mechanistic insight into the process. Our data demonstrating the affinity of PrP^{C} for iron raises several questions concerning PrP^{Sc} propagation and prion disease pathogenesis. It is evident that PrP^{C} changes to $*PrP^{Sc}$ when exposed to redox iron, an event most likely modulated by PrP^{C}-bound iron. Metals such as iron and copper are known to interact with specific proteins, and they are reduced in their presence, resulting in protein aggregation and concomitant generation of highly toxic reactive oxygen species, H_2O_2, and hydroxyl radical ($OH^{\cdot}$) (Behl *et al.*, 1994). Initiation of such a reaction between free radicals and PrP^{C}-bound iron could explain the conversion of PrP^{C} to PrP^{Sc}. Highly reactive radicals released during the process would account for the change of additional PrP^{C} to PrP^{Sc} and associated neurotoxicity. Our data demonstrating the generation of redox-active $*PrP^{Sc}$–ferritin

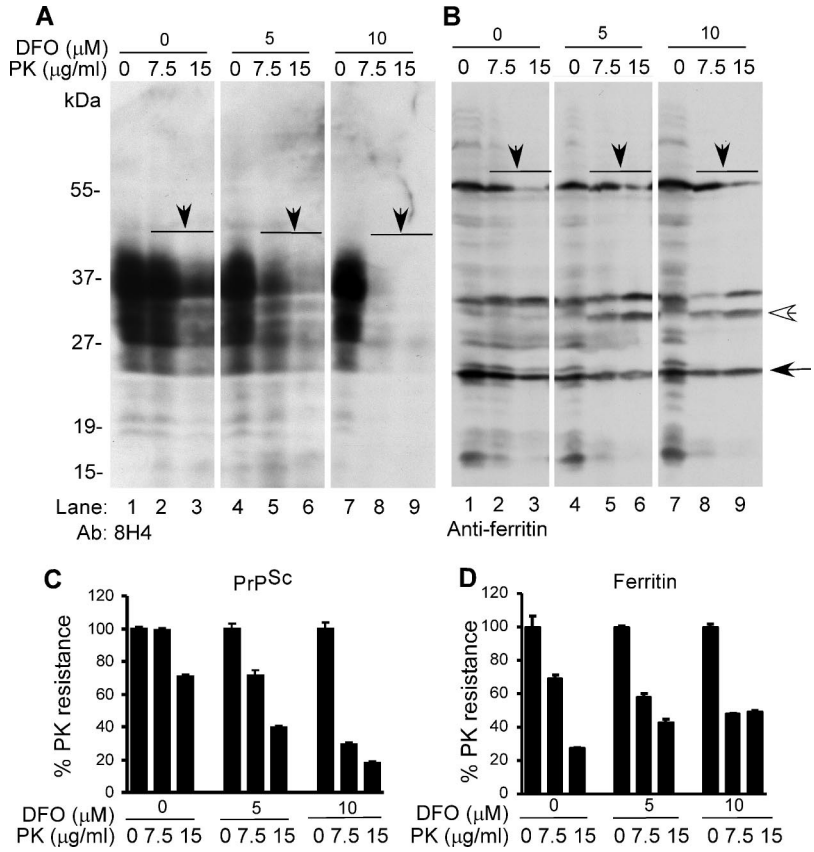

Figure 7. (A) ScN2a cells were cultured for 24 h in serum-free medium supplemented with vehicle or 5 and 10 μM DFO. (Notably, cells exposed to DFO looked healthier than untreated controls after 24 h.) Subsequently, cells were washed with PBS, and lysates were treated with vehicle or 7.5 and 15 μg/ml PK for 5 min at 37°C. Resistant proteins were recovered and immunoblotted with 8H4. Control sample without DFO and PK treatment shows the expected glycoforms of PrP (lane 1), some of which are degraded by PK treatment (lanes 2 and 3). Exposure to 5 and 10 μM DFO shows a significant decrease in PK-resistant PrP^{Sc}, more so in the latter sample (lanes 4–9). (B) Reprobing for ferritin shows limited sensitivity to PK regardless of DFO treatment (lanes 1–9). Certain oligomeric forms decrease in intensity (lanes 1–9, solid arrowheads), whereas others increase following PK treatment (lanes 1–9, white arrowhead). (C) Quantification shows a significant decline in PK-resistant PrP^{Sc} from 99 to 70% and from 70 to 40% with 7.5 and 15 μg/ml PK, respectively, after exposure to 5 μM DFO. A further decline in PK-resistant PrP^{Sc} to 30 and 18%, respectively, is observed when the DFO concentration is increased to 10 μM. n = 4. (D) The total amount of PK-resistant ferritin ranges between 75 and 95% regardless of DFO treatment. n = 4.

complexes by exposing PrP^{C} cells to $FeCl_2$ and generation of additional $*PrP^{Sc}$ by these complexes supports this hypothesis. Although the $*PrP^{Sc}$ induced by $FeCl_2$ shows 10-fold less PK resistance than brain-derived PrP^{Sc}, it resembles the latter in several biochemical and biophysical characteristics such as insolubility in nonionic detergents, generation of the typical 19- to 20-kDa C-terminal fragment on PK treatment, and nonreactivity with 3F4 unless denatured. It is notable that similar treatment of astrocytes that possess redox-shuttling proteins such as ceruloplasmin in their plasma membrane does not result in up-regulation or aggregation of PrP^{C} or ferritin in response to $FeCl_2$. Likewise, transfection of PrP^{C} cells with ceruloplasmin significantly reduces intracellular $*PrP^{Sc}$ (our unpublished observations), indicating that accumulation of $*PrP^{Sc}$ is a consequence of redox iron-mediated insult. The greater propensity for unglycosylated PrP to aggregate in response to $FeCl_2$ supports previous observations suggesting a protective role of glycans in preventing the conformational change of PrP^{C} to PrP^{Sc} (Lehmann and Harris, 1997). Although one may argue that redox iron levels in $FeCl_2$ far exceed those in prion-affected brains, it is notable that similar cleavage of PKCδ to its catalytically active fragment is observed under both conditions, and the total iron in $*PrP^{Sc}$ isolated from $FeCl_2$-exposed cells does not exceed the level in diseased brains significantly. Moreover, treated cells do not show any evidence of toxicity, and they revert back to normal morphology within 7 d of culture in normal medium, excluding direct toxicity as a cause of $*PrP^{Sc}$ formation. Similar doses of $FeCl_2$ have been used to demonstrate sensitivity of α-synuclein to oxidative stress in cell culture models (Ostrerova-Golts *et al.*, 2000), and other stressors such as H_2O_2 used at a concentration of 100–200 μM in experimental paradigms of oxidative damage to PrP^{C} have provided useful information (McMahon *et al.*, 2001; Turnbull *et al.*, 2003; Zeng *et al.*, 2003), reinforcing the biological relevance of our model. It is intriguing that depletion of iron from infectious brain homogenates reduces PK-resistant PrP^{Sc} 5- to 10-fold without altering ferritin levels. One plausible explanation for this result could be that the interaction of PrP^{Sc} and ferritin is mediated through iron, and the inherently PK-resistant nature of ferritin confers stability to associated PrP^{Sc} (Mishra *et al.*, 2004). We have observed relatively higher resistance of brain-derived ferritin to PK digestion compared with cellular ferritin, a fact that may explain the comparably higher PK resistance of brain PrP^{Sc} (100 μg/ml) compared with cell-associated PrP^{Sc} (15 μg/ml). Whether reduction of PK-resistant PrP^{Sc} by iron depletion will decrease infectivity of sCJD and mouse scrapie brain homogenates and ScN2a cells is unclear from our data, but copper chelation has been shown to delay disease onset in experimental mice (Sigurdsson *et al.*, 2003), providing optimism for iron chelation as a possible means for decreasing PrP^{Sc} load. Previous studies have unraveled important facts about the mechanism of PrP^{Sc} generation and propagation. For example, nonfibrillar PrP^{Sc} particles containing 14–28 molecules seem to be sufficient for efficient transmission of prion infectivity, although cell-specific factors are necessary for successful PrP^{Sc} propagation (Vorberg *et al.*, 2004; Magalhaes *et al.*, 2005; Bieschke *et al.*, 2004). Conversion of cellular, brain-derived, or recombinant PrP^{C} to a PrP^{Sc}-like form has been achieved in vitro by incubation with brain-derived infectious PrP^{Sc}, RNA molecules, redox-active metals such as copper, certain denaturants, solvents, pH and temperature conditions, reducing agents, inhibition of glycosylation, by the protein misfolding cyclic amplification reaction, and a combination of buffer conditions and metal ions (Brown *et al.*,

2000; Qin *et al*., 2000; Nishina *et al*., 2004; Castilla *et al*., 2005; Kim *et al*., 2005). Our report extends these studies by generating a PrP^{Sc}-like molecule in a biologically relevant ex vivo model by using doses of redox iron that are close to the levels detected in prion-infected brains. Moreover, similar doses of $FeCl_2$ when added to cell lysates do not induce a change in conformation of PrP^{C} to $*PrP^{Sc}$ (our unpublished observations), implicating cellular factors and/or signaling pathways in the process, not a simple chemical or a biophysical reaction. Whether the observed effects are due to redox cycling of metal ions in general, including copper, or they are specific to iron remains to be determined. Although our hypothesis implicating redox iron as a major trigger for PrP^{Sc} propagation answers only some pieces of the prion puzzle, the significance and novelty of the data far exceed its shortcomings and lay the foundation for further investigations on the role of brain iron homeostasis in prion disease pathogenesis, and iron chelation as a potential strategy for reducing PrP^{Sc} load.

ACKNOWLEDGMENTS

We thank Dr. Surewicz for providing recombinant PrP, Drs. Raymond and Caughey for providing scrapie-infected neuroblastoma cells, Dr. Gambetti for normal and sCJD brain tissue, Drs. Sy and Gambetti for anti-PrP antibody 8H4, and Yaping Gu and Yugarshi Mondal for help in the preparation of the manuscript. This study was supported by National Institutes of Health grants NS-39089 and NS-35962 (to N.S.).

REFERENCES

Aguzzi, A., and Polymendiou, M. (2004). Mammalian prion biology: one century of evolving concepts. Cell *116*, 313–327.

Andreoletti, O., Levavasseur, E., Uro-Coste, E., Tabouret, G., Sarradin, P., Delisle, M. B., Berthon, P., Salvayre, R., Schelcher, F., and Negre-Salvayre, A. (2002). Astrocytes accumulate 4-hydroxynonenal adducts in murine scrapie and human Creutzfeldt-Jakob disease. Neurobiol. Dis. *11*, 386–393.

Behl, C., Davis, J. B., Lesley, R., and Schubert, D. (1994). Hydrogen peroxide mediates amyloid beta protein toxicity. Cell *77*, 817–827.

Bieschke, J., Weber, P., Sarafoff, N., Beekes, M., Giese, A., and Kretzschmar, H. (2004). Autocatalytic self-propagation of misfolded prion protein. Proc. Natl. Acad. Sci. USA *101*, 12207–12211.

Brazier, M. W. *et al*. (2006). Correlative studies support lipid peroxidation is linked to PrP(res) propagation as an early primary pathogenic event in prion disease. Brain Res. Bull. *68*, 346–354.

Brown, D. R., Hafiz, F., Glasssmith, L. L., Wong, B-S., Jones, I. M., Clive, C., and Haswell, S. J. (2000). Consequences of manganese replacement of copper for prion protein function and proteinase resistance. EMBO J. *19*, 1180–1186.

Castilla, J., Saa, P., Hetz, C., and Soto, C. (2005). In vitro generation of infectious scrapie prions. Cell *121*, 195–206.

Chesebro, B. *et al*. (2005). Anchorless prion protein results in infectious amyloid disease without clinical scrapie. Science *308*, 1435–1439.

Chiesa, R., and Harris, D. A. (2001). Prion diseases: what is the neurotoxic molecule? Neurobiol. Dis. *8*, *743–763*.

Fernaeus, S., and Land, T. (2005). Increased iron-induced oxidative stress and toxicity in scrapie-infected neuroblastoma cells. Neurosci. Lett. *382*, 133–136.

Harris, D. A., and True, H. L. (2006). New insights into prion structure and toxicity. Neuron *50*, 353–357.

Hur, K., Kim, J. I., Choi, S. I., Choi, E. K., Carp, R. I., and Kim, Y. S. (2002). The pathogenic mechanisms of prion diseases. Mech. Ageing Dev. *123*, 1637–1647.

Kaul, S., Kanthasamy, A., Kitazawa, M., Anantharam, V., and Kanthasamy, A. G. (2003). Caspase-3 dependent proteolytic activation of protein kinase C delta mediates and regulates 1-methyl-4-phenylpyridinium (MPP+)-induced apoptotic cell death in dopaminergic cells: relevance to oxidative stress in dopaminergic degeneration. Eur. J. Neurosci. *18*, 1387–1401.

Kim, N. H., Choi, J. K., Jeong, B. H., Kim, J. I., Kwon, M. S., Carp, R. I., and Kim, Y. S. (2005). Effect of transition metals (Mn, Cu, Fe) and deoxycholic acid (DA) on the conversion of PrPC to PrPres. FASEB J. *19*, 783–785.

Kim, N. H., Park, S. J., Jin, J. K., Kwon, M. S., Choi, E. K., Karp, R. I., and Kim, Y. S. (2000). Increased ferric iron content and iron-induced oxidative stress in the brains of scrapie-infected mice. Brain Res. *884*, 98–103.

Lasmezas, C. I., Deslys, J. P., Robain, O., Jaegly, A., Beringue, V., Peyrin, J. M., Fournier, J. G., Hauw, J. J., Rossier, J., and Dormont, D. (1997). Transmission of the BSE agent to mice in the absence of detectable abnormal prion protein. Science *275*, 402–405.

Lehmann, S., and Harris, D. A. (1997). Blockade of glycosylation promotes acquisition of scrapie-like properties by the prion protein in cultured cells. J. Biol. Chem. *272*, 21479–21487.

Magalhaes, A. C., Baron, G. S., Lee, K. S., Steele-Mortimer, O., Dorward, D., Prado, M. A., and Caughey, B. (2005). Uptake and neuritic transport of scrapie prion protein coincident with infection of neuronal cells. J. Neurosci. *25*, 5207–5216.

Mallucci, G., Dickinson, A., Linehan, J., Klohn, P. C., Brandner, S., and Collinge, J. (2003). Depleting neuronal PrP in prion infection prevents disease and reverses spongiosis. Science *302*, 871–874.

McMahon, H. E., Mange, A., Nishida, N., Creminon, C., Casanova, D., and Lehmann, S. (2001). Cleavage of the amino terminus of the prion protein by reactive oxygen species. J. Biol. Chem. *276*, 2286–2291.

Mishra, R. S. *et al*. (2004). Protease-resistant human prion protein and ferritin are co transported across Caco-2 epithelial cells: implications for species barrier in prion uptake from the intestine. J. Neurosci. *24*, 11280–11290.

Morillas, M., Swietnicki, W., Gambetti, P., and Surewicz, W. K. (1999). Membrane environment alters the conformational structure of the recombinant human prion protein. J. Biol. Chem. *274*, 36859–36865.

Nishina, K., Jenks, S., and Supattapone, S. (2004). Ionic strength and transition metals control PrPSc protease resistance and conversion-inducing activity. J. Biol. Chem. *279*, 40788–40794.

Ostrerova-Golts, N., Petrucelli, L., Hardy, J., Lee, J. M., Farer, M., and Wolozin, B. (2000). The A53T alpha-synuclein mutation increases iron-dependent aggregation and toxicity. J. Neurosci. *20*, 6048–6054.

Patel, B. N., and David, S. (1997). A novel glycosylphosphatidylinositol-anchored form of ceruloplasmin is expressed by mammalian astrocytes. J. Biol. Chem. *272*, 20185–20190.

Petersen, R. B. *et al*. (2005). Redox metals and oxidative abnormalities in human prion diseases. Acta Neuropathol. *110*, 232–238.

Prusiner, S. B. (1998). Prions. Proc. Natl. Acad. Sci. USA *95*, 3363–3383.

Qin, K., Yang, D. S., Yang, Y., Chishti, M. A., Meng, L. J., Kretzschmar, H. A., Yip, C. M., Fraser, P. E., and Westaway, D. (2000). Copper(II)-induced conformational changes and protease resistance in recombinant and cellular PrP. Effect of protein age and deamidation. J. Biol. Chem. *275*, 19121–19131.

Sigurdsson, E. M., Brown, D. R., Alim, M. A., Scholtzova, H., Carp, R., Meeker, H. C., Prelli, F., Frangione, B., and Wisniewski, T. (2003). Copper chelation delays the onset of prion disease. J. Biol. Chem. *278*, 46199–46202.

Singh, N., Zanusso, G., Chen, S. G., Fujioka, H., Richardson, S., Gambetti, P., and Petersen, R. B. (1997). Prion protein aggregation reverted by low temperature in transfected cells carrying a prion protein gene mutation. J. Biol. Chem. *272*, 28461–28470.

Smith, M. A., Harris, P. L., Sayre, L. M., and Perry, G. (1997). Iron accumulation in Alzheimer disease is a source of redox-generated free radicals. Proc. Natl. Acad. Sci. USA *94*, 9866–9868.

Taraboulos, A., Rogers, M., Borchelt, D. R., McKinley, M. P., Scott, M., Serban, D., and Prusiner, S. B. (1990). Acquisition of protease resistance by prion proteins in scrapie-infected cells does not require asparagine-linked glycosylation. Proc. Natl. Acad. Sci. USA *87*, 8262–8266.

Thackray, A. M., Knight, R., Haswell, S. J., Bujdoso, R., and Brown, D. R. (2002). Metal imbalance and compromised antioxidant function are early changes in prion disease. Biochem. J. *362*, 253–258.

Thompsett, A. R., Abdelraheim, S. R., Daniels, M., and Brown, D. R. (2005). High affinity binding between copper and full-length prion protein identified by two different techniques. J. Biol. Chem. *280*, 42750–42758.

Turnbull, S., Tabner, B. J., Brown, D. R., and Allsop, D. (2003). Generation of hydrogen peroxide from mutant forms of the prion protein fragment PrP121-231. Biochemistry *42*, 7675–7681.

Vorberg, I., Raines, A., and Priola, S. A. (2004). Acute formation of protease-resistant prion protein does not always lead to persistent scrapie infection in vitro. J. Biol. Chem. *279*, 29218–29225.

Vyoral, D., Petrak, J., and Hradilek, A. (1998). Separation of cellular iron containing compounds by electrophoresis. Biol. Trace Elem. Res. *61*, 263–275.

Wong, B. S. *et al*. (2001). Increased levels of oxidative stress markers detected in the brains of mice devoid of prion protein. J. Neurochem. *76*, 565–572.

Zeng, F., Watt, N. T., Walmsley, A. R., and Hooper, N. M. (2003). Tethering the N-terminus of the prion protein compromises the cellular response to oxidative stress. J Neurochem *84*, 480–490.